FACILE SYNTHESIS AND LUMINESCENE PROPERTIES OF $CePO_4$: Tb^{3+} BY ELECTROSPINNING

Q. LI[a*], Z. P. LIU[a] , L. M. DONG[a], Y. F. ZHANG[b]
[a]*College of Materials Science and Engineering, Harbin University of Science & Technology Harbin, China*
[b]*AECC Harbin Dongan Engine Co.,LTD. , Harbin, China*

A series of single-phase $CePO_4$: Tb^{3+} luminescent material was prepared by electrospinning method, and $CePO_4$: Tb^{3+} phosphor was obtained after further calcination. Thermogravimetric differential thermal analysis (TG-DTA) was used to analysis the formation of nano-fibers from the precursor, X-ray powder diffraction was used to analysis crystal structure of the material; Scanning electron microscopy was used to characterize the morphology of the material, and fluorescence spectroscopy was used to analysis fluorescence properties of the material. The obtained phosphors can be efficiently excited in the range from 340 to 385 nm. Under 377 nm excitation, the $CePO_4$: Tb^{3+} phosphors emit intense green light at 542nm due to the $^5D_4 \rightarrow {}^7F_5$ electric dipole transition of Tb^{3+} ions.

(Received September 22, 2016, Accepted December 5, 2016)

Keywords: Cerous phosphate phosphor, Fluorescent properties, Electrospinning method

1. Introduction

Nowadays, trivalent rare-earth ions (RE^{3+}) activated inorganic compounds have attracted a lot of research attention due to their potential applications in light-emitting diodes (LEDs), fluorescent lamps, flat plane displays, solid state laser and high energy radiation detectors [1–3]. Many inorganic compounds such as phosphate [4], silicate [5], aluminate [6] and borate [7] doped with RE^{3+} ions (Tb^{3+}, Eu^{3+}, Pr^{3+}, Sm^{3+}, Tm^{3+}) were extensively studied as phosphors, due to their efficient visible emissions under near-UV (NUV) excitation. Among these applications, phosphor are important candidates for solid state lighting in converting white light emitting diodes (pc - WLEDs) because of their excellent properties, such as long operational lifetime, energy saving, high brightness, higher luminescent efficiency, compactness, and environment friendliness [8,9]. Morphology of phosphors is also one of the key parameters of their industrial application.

1D and Q-1D nanomaterials with different compositions have been developed using various methods including chemical or physical vapor deposition, laser ablation, solution, arc discharge, vapor-phase transport process, and a template-based method [10-15]. Compared to these methods, electrospinning is a simple, convenient, cost-effective, and versatile technique for generating long fibers with diameters ranging from tens of nanometers up to micrometers. The fibers prepared by electrospinning have good orientation, a large specific surface area, a large aspect ratio, and dimensional stability, which can be applied in sensors, electronic and optical devices, biomedical fields, and catalyst supports [16].

Lanthanide orthophosphates ($LnPO_4$) belong to two polymorphic types, the monoclinic monazite type (for La to Gd) and the quadratic xenotime type (for Tb to Lu). Cerium phosphate ($CePO_4$) has been shown to be a useful host lattice for rare earth ions to produce phosphors emitting a variety of colors. In comparison with bulk materials, the shape anisotropy of a 1D structure provided a better model system to investigate the dependence of electronic transport and

* Corresponding author. qinalily@163.com

optical properties on size confinement and dimensionality.

The luminescent $CePO_4$: Tb (rare earth) 1D nanocrystals have also attracted considerable interest [17-19]. As far as we know, no series of Tb^{3+} doped $CePO_4$ nanofiber has been prepared by electrospinning method. Herein, a series of Tb^{3+} doped $CePO_4$ nanofiber has been synthesized by electrospinning methods and their structure and luminescence properties were investigated in detail.

2. Materials and methods

2.1. Materials Preparation

All of the chemical reagents used in this experiment were analytical grade. According to a certain proportion weighed amount, $NH_4H_2PO_4$ and $Ce(NO_3)_3 \cdot 6H_2O$ were dissolved in an appropriate amount of distilled water, and Tb_4O_7 dissolved in an appropriate amount of nitric acid, then the above solutions were mixed. Citric acid was slowly added to the mixing solutions, after which ethanol and polyvinyl pyrrolidone was added to the solution, and stirred again for 4 h at room temperature, to achieve a homogenous solution. The parameters of electrospinning were set to draw good nano-fibers through an optimization process. The drum collector separated from the needle by 15 cm. The voltage maintained between the needle and collector was 30 kV. After electrospinning, the precursor was calcinated in the temperature range 1000–1300 °C for 4 h in a high-temperature resistance furnace.

2.2. Analysis Methods

The structures of the phosphor were established by X-ray diffractometer (XRD) (Shimadzu, XRD-6000, Cu Ka target) and the morphology of the particles was observed by field emission scanning electron microscope (FE-SEM) (Sirion 200, Philip). Thermogravimetric and differential thermal analysis (TG–DTA) data were recorded with a thermal analysis instrument (TA SDT N5350030), with a heating rate of 10 °C/min. The photoluminescence properties of the phosphors were studied on fluorescence spectrophotometer (Shimadzu, model RF-5301 PC). All the photoluminescence properties of the phosphors were measured at room temperature.

3. Results and discussion

3.1 Phase Identification and Crystal Structure.

The phase composition and purity of the as-prepared powder samples were detected by XRD. Fig. 1 shows the representative XRD patterns for $CePO_4$: $0.08Tb^{3+}$ samples. It shows that all the diffraction peaks match well with that of standard JCPDS card (No. 32−247); and no other phase of the peak were detected, indicating the prepared samples were single phase. According to the XRD patterns, we can deduce that the Tb^{3+} ions were completely dissolved in the $CePO_4$ host without inducing significant changes of the crystal structure. The $CePO_4$: $0.08Tb^{3+}$ crystallizes in the monoclinic space group P21/n(14) with cell parameters of a = 6.789Å, b = 7.013Å, c =6.469Å.

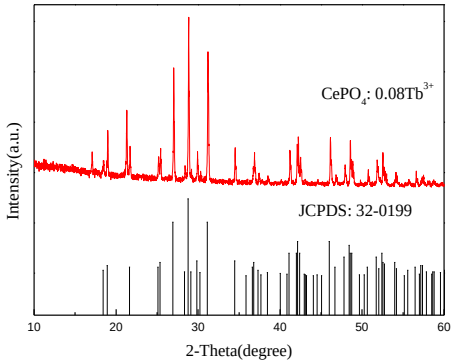

Fig. 1: Representative XRD patterns of Tb^{3+} doped $CePO_4$ samples synthesized at 1100°C for 4h. The reference is standard card data of $CePO_4$ (JCPDS Card No. 32−0199) is shown as a reference.

In order to investigate the effect of calcination temperature on luminescence properties, a series of $CePO_4$: $0.08Tb^{3+}$ phosphors were obtained after sintering at different temperature. Figure 2 shows the XRD patterns of $CePO_4$: $0.08Tb^{3+}$ after calcination at different temperatures ranging from 900°C to 1300°C for 4h in air. From figure 2 we can see all of the patterns are similar. When the calcination temperature is 900°C and 1000°C, the sample diffraction peak is weak, and it is due to that the energy required for the crystal growth is not sufficient, which leads to the crystal growth is not complete. When the calcination temperature is 1100°C, the diffraction peak is sharp and consistent with the standard XRD pattern, indicating that the crystal growth was complete. At higher calcination temperature (1200°C and 1300°C), the intensity of the diffraction peak appears to decrease slightly, which indicates that the crystal growth of the material can be influenced when the temperature is too high.

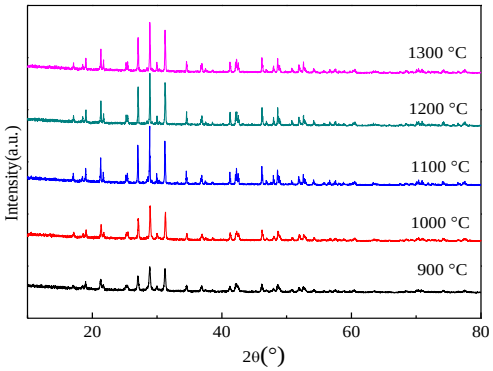

Fig. 2: XRD spectra of $CePO_4$: Tb^{3+} at different calcination temperatures

3.2 Thermal Analysis

The TG–DTA curves of the as-spun composite fibers heated in air are shown in figure 3. The TG curves show that most of the organic materials and volatiles were removed under 1000 °C. Four discrete regions of weight loss occurred at about 120,140, 360 and 460 °C, respectively. The endothermic region in the DTA curve at a temperature about 120 °C indicates the evaporation of moisture and ethyl alcohol. The peaks at 140 and 360 °C of the DTA curve correspond to the decomposition of nitrate and degradation of PVP, respectively. The exothermic peak at 460 °C is due to the carbon and carbon oxide released by PVP [20]. At the temperature where the peak appears in the DTA curve, a drastic decrease of the TGA curve is also observed. This indicates the

evaporation and degradation of organic materials. Up to the temperature of 800 °C, the weight loss appeared to be continuous. Through this decreasing weight in the TGA curve, we can easily assume that the most organic materials are decomposed, and $CePO_4$: Tb^{3+} was synthesized.

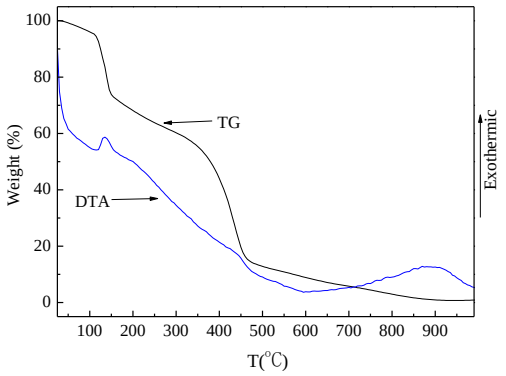

Fig. 3. TG-DTA curves of $CePO_4$: Tb^{3+} as-spun precursor.

3.3 SEM Images

The SEM images of these precursor fibers and the resulted $CePO_4$: Tb^{3+} after calcination are shown in figure 4(a)–(b). As shown in figure 4(a), $CePO_4$: Tb^{3+} fiber precursor is in uniform thickness, the surface was very smooth and no adhesion appears, the diameter was about 6 μm. Figure 4(b) is the SEM image of $CePO_4$: Tb^{3+} calcined at 1100 ^oC. From the picture, we can see that the surface becomes rough and the occurrence of adhesions, fibers shrink curved significantly and appeared broken. It appears to be connected by the fine particles formed. The main reason is that in the sample after calcination, volatiles of deionized water and absolute ethanol, and decomposition of polyvinylpyrrolidone lead to a significant decrease in the diameter of the sample, the diameter is about 300 nm, the $CePO_4$: Tb^{3+} shows the shape in short rod.

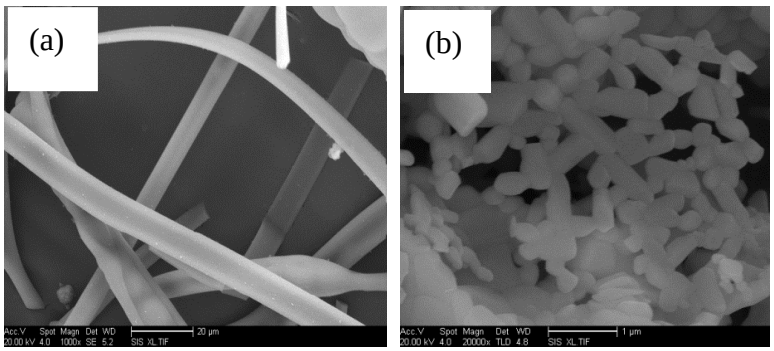

Fig. 4: SEM images of as-spun precursor for $CePO_4$: Tb^{3+} nano-fibers images (a) and annealed at 1100°C (b)

3.4 Optical Comparisons

Fig. 5 shows the photoluminescence (PL) and photoluminescence excitation (PLE) spectra of $CePO_4$: $0.08Tb^{3+}$. The excitation spectrum (figure 5, left), which is recorded by monitoring with green emission peak at 542 nm, reveals a series of spectral bands in the range of 345–400 nm. The sharp excitation peaks could be appropriately attributed to Tb^{3+} 4f-4f forbidden transitions. And the peaks are resulted from the transitions of $^7F_6$-$^5D_2$ (351 nm) and $^7F_6$-$^5G_6$ (370 and 377 nm) [21]. Among these excitation peaks, the most prominent peak at 377 nm is chosen to pump for which strong emission, this is mainly due to the 5d orbit of Tb^{3+} exposed outside, and the surrounding

environment will have a strong effect on the 5d electrons in the outer layer, which can cause the energy level of 5d to be split. At the same time, it can be seen that the fluorescent powder can be well matched with the commercial positive UV LED chip (360- 410 nm) [22].

In emission spectrum (Fig. 5, right), the peaks arising in the green region at 491 nm, 542 nm, 585 nm, and 624 nm are assigned to $^5D_4$-^7F_J (J=6, 5, 4, 3) transitions, respectively. In agreement with the selection rule $\Delta J=\pm 1$, Laporte's forbidden transition of $^5D_4$-$^7F_5$(542 nm) showed bright green emission, and it has the strongest intensity and largest probability for electric-dipole transition.

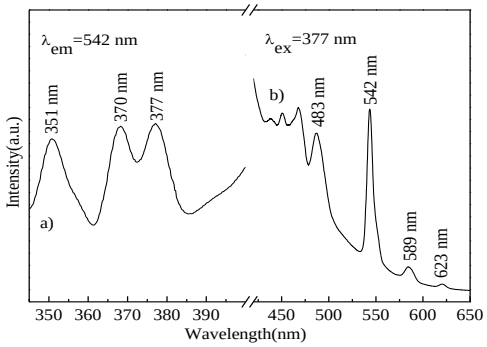

Fig. 5: PL and PLE spectra of $CePO_4$: $0.08Tb^{3+}$ phosphor

In order to investigate the effect of doping concentration on luminescence properties, a series of $CePO_4$: xTb^{3+} (x=0.02, 0.04, 0.06, 0.08, 0.10) phosphors were synthesized. Figure 6 shows the PL spectra of $CePO_4$: xTb^{3+} with different doping contents. The green emission of the Tb^{3+} increases gradually and reaches a maximum at x= 0.08. With further increment of Tb^{3+} concentration, the emission intensity begins to decrease due to concentration quenching. According to the Dexter's energy transfer theory [23], concentration quenching is mainly caused by the nonradiative energy migration among the Tb^{3+} ions at the high concentration.

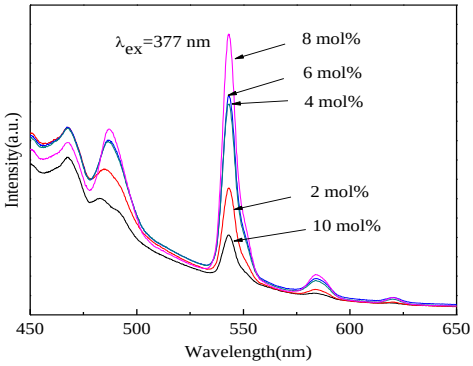

Fig. 6: The emission spectra of $CePO_4$: Tb^{3+} with different Tb^{3+} doping amounts

Fig. 7 shows the PL spectra of $CePO_4$: $0.08Tb^{3+}$ at different calcination temperatures. Comparably, all of the emission spectra of $CePO_4$: $0.08Tb^{3+}$ is quite similar from each other. With the increase of the calcination temperature, the luminescence intensity showed an upward trend below 1100°C. However, the calcination temperature is above 1100°C, the luminous intensity then decreases sharply. The luminous intensity reaches the maximum at 1000°C. This is mainly because when the temperature is too high, over sintering phenomenon will appear. This is consistent with the result form figure 2. From the above analysis, it can be concluded that it is very important to select the appropriate calcination temperature and the best calcination temperature is 1100°C.

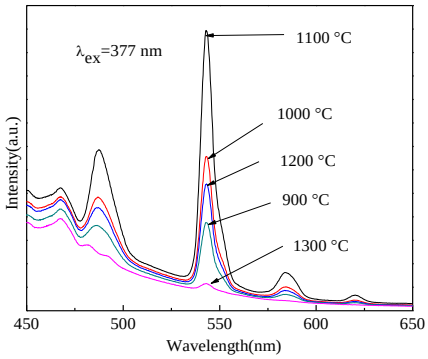

Fig. 7: Emission spectra of $CePO_4$: $0.08Tb^{3+}$ at different calcination temperatures

4. Conclusions

In summary, a green-emitting phosphor $CePO_4$: Tb^{3+} was synthesized by the electrospinning method, the photoluminescence properties and crystal structure was investigated. The $CePO_4$ crystallizes in the monoclinic space group P21/n(14). The obtained phosphors can be effciently excited in the range from 340 to 385 nm, Under 377 nm excitation, the $CePO_4$: Tb^{3+} phosphors emit intense green light at 542nm due to the $^5D_4 \rightarrow {}^7F_5$ electric dipole transition of Tb^{3+} ions, and the optimal calcination temperature is 1100 ^oC and the optimal concentration of the Tb^{3+} is 8 mol%.

Acknowledgment

This work was financially supported by special fund project for science and technology innovation talents of Harbin (2016RQQXJ137).

References

[1] C. Guo, H. Jing, T. Li, RSC Adv. **2**, 2119 (2012).
[2] M. Xie, C. Luo, Phys. Status Solidi (RRL) **6**, 412 (2012).
[3] I. Valais, C. Michail, S. David, et al., Phys. Med. **24**,122 (2008).
[4] G. Dong, H. Ma, Y. Liu, Z. Yang, Q. Liu, Opt. Commun. **285,** 4097 (2012).
[5] Y. Chen, M. Gong, K.W. Cheah, Mater. Sci. Eng. B **166**, 24 (2010).
[6] X. Chen, J. Zhao, L. Yu, C. Rong, C. Li, S. Lian, J. Lumin. **131**, 2697 (2011).
[7] F. Yang, Y. Liang, Y. Lan, W. Gao, M. Liu, X. Li, W. Huang, Z. Xia, Mater. Lett. **83**, 59 (2012) .
[8] C.C. Lin, R.S. Liu, J. Phys. Chem. Lett. **2**, 1268 (2011).
[9] S. Ye, F. Xiao, Y.X. Pan, et al., Mater. Sci. Eng. R. **71**,1 (2010).
[10] S.Y. Bae, H.W. Seo, J. Park, H. Yang, J.C. Park, S.Y. Lee, Appl. Phys. Lett. **81**, 126 (2002).
[11] L. Fu, Y.Q. Liu, P. Hu, K. Xiao, G. Yu, D.B. Zhu, Chem. Mater. **15**, 4287 (2003).
[12] X.F. Duan, C.M. Lieber, Adv. Mater. **12**, 298 (2000).
[13] J.H. Jung, H. Kobayashi, B. Van, S. Shinkai, T. Shimizu, Chem. Mater. **14**, 1445 (2002).
[14] Y. Wu, P. Yang, Chem. Mater. **12**, 605 (2000).
[15] M.H. Huang, A. Choudrey, P. Yang, Chem. Commun. **12**, 1063 (2000).
[16] L. Pieterson, S. Soverna, A. Meijerink, J Electrochem Soc., **147**, 4688 (2000).
[17] K. Riwotzki, H. Meyssamy, A. Kornowski, M.Haase, .J.Phys.Chem.B. **104**, 2824 (2000).
[18] M. Guan, J. Sun, M. Han, Z. Xu, F. Tao, G. Yin, X. Wei, J. Zhu, X.Jiang, .Nanoteclmology.

18, 415602 (2007).
[19] Q. Li, V.W.-W. Yam, Angew.Chem.Int.Ed. **46**, 3486 (2007)..
[20] W. Liu, C. Wang, Indian J Chem A Inorg Bioinorg Phys Theor Anal Chem **49**, 307 (2010).
[21] X. Zhou, Z. Zhang, Y. Wang, J. Mater. Chem. C **3**, 3676 (2015).
[22] M. Jiao, N. Guo, W. Lu, et al., Inorganic Chemistry **52**, 10340 (2013).
[23] D.Dexter, J. H. Schulman, J. Chem. Phys. **22**, 1063 (1954).